Modelling the precipitation of nanoparticles in a closed medium in the presence of seeds: Application to amorphous silica synthesis

Claudine Noguera, Bernard Fritz, Alain Clément, Damien Lemarchand

Modelling the precipitation of nanoparticles in a closed medium in the presence of seeds: Application to amorphous silica synthesis.

C. Noguera,[1] B. Fritz,[2] A. Clément,[2] and D. Lemarchand[2]

[1] *CNRS-Sorbonne Université, UMR 7588, INSP, 4 Place Jussieu, F-75005 Paris, France*
[2] *Université de Strasbourg/EOST,CNRS, Laboratoire d'Hydrologie et de Géochimie de Strasbourg, 1 rue Blessig, Strasbourg Cedex F-67084, France*

(Dated: March 9, 2021)

Seed-mediated methods are widely used in industrial or academic laboratories for the synthesis of nanoparticles of controlled shape and size. In the natural medium, precipitation of secondary minerals also often take place on seeds. In this context, we have devised a formalism which accounts for the competition between seed growth and nucleation and growth of secondary particles in an initially over-saturated aqueous solution. Based on the classical nucleation theory, it involves a size-dependent growth law which accounts for Ostwald ripening effects, unlike most water-rock interaction codes. We find that, in such closed system, seed growth and nucleation/growth of secondary particles are strongly coupled. In the multi-dimensional parameter space, regions where one or the other process prevails are well-separated by a rather abrupt transition. In general, the value of the initial seed total surface area is insufficient to fully orientate the synthesis. Relying on this approach, we propose an alternative interpretation of recent experimental results on amorphous silica nanoparticle synthesis. Besides fundamental understanding of the kinetics of precipitation, the interest of the present approach is to serve as a guideline to experimentalists or industrialists working in seed-mediated syntheses and warn on the undesired formation of secondary particles when monodispersed distributions of nano- or micro-particles are searched.

Keywords: seed-mediated synthesis, water-rock interaction, amorphous silica, dissolution, nucleation and growth, computer simulation, Nanokin code

Highlights:

- A formalism is devised which accounts for both seed growth and formation of secondary particles in an initially over-saturated aqueous solution.
- Seed growth and nucleation/growth of secondary particles are strongly coupled and prevail in separate regions of the kinetic parameter values.
- An alternative interpretation of recent experimental results on amorphous silica nanoparticle synthesis is proposed.

PACS numbers:

I. INTRODUCTION

In the last decades, micro- and nanoparticles (NPs) have become ubiquitous in various fields of research—physics (e.g. plasmonics), chemistry (e.g. catalysis), geosciences (e.g. transport of nutrients and pollutants[1])—or applications. With the advent of nanotechnology, methods of fabrication of ultra-fine particles with efficient size and shape control have been developed. This concerns, for example, the fabrication of pigments used in the food industry, the particles used in the pharmaceutical industry[2,3] or oxide-based catalysts with large surface-to-bulk ratio, used in acid-base reactions, gas phase partial oxidation reactions or combustion and depollution processes[4]. Gold or silver NPs have also received much attention due to their plasmonic properties and potential applications in chemical sensing, biological imaging, drug delivery and phototherapeutics[5].

NPs present a large spectrum of atomic and electronic structures, due to their finite size in the three dimensions of space and the fact that their atoms are nearly all surface atoms. Their composition, morphology and size influence their physical, chemical, optical, electronic and catalytic properties. For example, the variability of optical properties as a function of electron confinement and/or NP morphology has been demonstrated in metallic NPs[5], but also in the large variety of ZnO nano-objects[6] envisioned in a new generation of devices.

Wet-chemistry is a flexible synthesis approach, because of its relative simplicity and its use of inexpensive materials[7]. In a number of cases, it proceeds via the formation of precursors or seeds under specific conditions prior to the synthesis of the desired object. Seed-mediated methods have indeed often been used to obtain monodispersed or shape-selected particles—as in the case of gold NPs[8,9]—or simply because it accelerates the growth kinetics by providing reactive surfaces for the nucleation of secondary particles[10,11]. Examples scan a wide range of applications, including, among others, the precipitation of phosphate minerals onto magnetite seeds[12], formation of calcium oxalate crystals using cal-

cite seeds[13], the selective formation of zeolites from coal fly ash[14], industrial applications of nucleation seeding in the field of green cements hydration[15], or formation of amorphous silica NPs[10,11,16,17].

When seeds of the same mineral as the targeted NPs are used, their growth under over-saturation conditions may be concomitant with the formation of secondary particles, causing an eventual multimodal distribution of particle sizes. If the aim is to prepare monodispersed particles, adjustments of the reaction conditions are necessary to prevent the formation of these unintended particles[16,17]. A simple idea would be to increase the growth rate by a higher over-saturation, but this would also be accompanied by an increase in the nucleation rate of secondary particles. Whether in the lab, industry or in the natural medium, a better understanding of the competition between seed growth and nucleation of secondary particles thus appears necessary to better master the final product.

To describe the precipitation kinetics, several empirical approaches have been used in the past such as simplified rate equations[18–20], the Johnson–Mehl–Avrami–Kolmogorov model[21–25] or the Chronomal approach[24–26]. In our previous works, we have demonstrated that the use of the classical nucleation theory and of a size dependent growth law, as embedded in the NANOKIN code[27–29], allows a full description of precipitation processes in a closed system, including the time evolution of the aqueous solution composition and of the size distribution of the precipitated particles. Mineral transformation and solution evolution, in relation with experimental studies, have been illustrated in the hydrothermal carbonation of portlandite[30], the formation of amorphous silica particles[31], or the kinetics of precipitation of lizardite and magnesite from olivine alteration[32].

However, to the best of our knowledge, none of these approaches consider seed-driven precipitation. It is the aim of the present work to extend our previous formalism to describe the precipitation of a given mineral from an over-saturated solution, in the presence of seeds of the same mineral. We show that the two processes of seed growth and production of secondary particles are in competition and are partly mutually exclusive. We derive growth diagrams as a function of the various kinetic parameters involved and discuss the influence of the seed characteristics. We finally apply our formalism to the precipitation of amorphous silica particles and propose an alternative interpretation of recent experimental results[10,11].

The paper is organized as follows: after a description of the simulation method in Section II, we analyse the characteristics of seed growth and precipitation of secondary particles when they occur independently (Section III) or together (Section IV). After a discussion which addresses various issues raised by these simulations (Section V), we focus on the precipitation of amorphous silica particles in the presence of silica seeds under recent experimental conditions (Section VI).

II. SIMULATION METHOD

This section provides a formalism for the precipitation of a mineral of solubility product K, in a closed aqueous medium as a result of an initial over-saturation I_0[28,29]. The latter is defined as the ratio between the ionic activity product and the solubility product of the mineral. All properties, including the concentrations of aqueous species, are assumed to be homogeneous throughout the system. In view of application to amorphous silica precipitation, the formalism is described for spherical nanoparticles.

The account of nucleation relies on the classical theory of nucleation, valid at small or moderate over-saturation[33,34], in which the variation ΔG of the Gibbs' free energy for the condensation of n monomers (or 'growth units') of radius ρ reads (k_B the Boltzmann constant, T the temperature, and σ the mean surface energy):

$$\Delta G = -nk_BT\ln I + 4\pi\rho^2\sigma \tag{1}$$

For $I > 1$, ΔG displays a maximum ΔG^* as a function of n which defines the characteristics of the *critical nuclei*, whose size n^* and radius ρ^* are equal to (v the molecular volume in the bulk mineral):

$$\begin{aligned} n^* = \tfrac{2u}{\ln^3 I} \qquad \rho^* = \tfrac{w}{\ln I} \\ \text{with} \qquad u = \tfrac{16\pi\sigma^3 v^2}{3(k_BT)^3} \qquad w = \tfrac{2\sigma v}{k_BT} \end{aligned} \tag{2}$$

By inverting the Gibbs-Thomson equation $\rho^* = \frac{w}{\ln I}$, the effective saturation state of the solution in equilibrium with a particle of radius ρ is found equal to $\exp(w/\rho)$. This is equivalent to saying that the solubility product of a particle of radius ρ is increased by this same amount, compared to infinitely large particles[35]. This effective size-dependent solubility product allows some particles to be supercritical while some others are under-critical for a same value of the saturation state I (Ostwald ripening effect, see below).

The nucleation barrier ΔG^*:

$$\Delta G^* = k_BT\frac{u}{\ln^2 I} = \frac{1}{3}4\pi\rho^{*2}\sigma \tag{3}$$

is inversely proportional to the square of $\ln I$ and equal to one-third of the total surface energy of the critical nucleus. The nucleation frequency (number of nucleated particles per second and litre of aqueous solution) exponentially depends on ΔG^*:

$$F = F_0\exp\left(-\frac{\Delta G^*}{k_BT}\right) \tag{4}$$

There have been multiple attempts to relate the prefactor F_0 to microscopic quantities, such as the diffusion coefficient, the Zeldovich factor and the monomer concentration[34]. However, in most cases, they have led to huge discrepancies with experimental results. With

respect to the monomer concentration, a linear relationship is proposed by some authors[34,36], but the highly non-linear relationship between F and I is essentially driven by the exponential term $\exp(-\Delta G^*/k_BT) = \exp(-u/\ln^2 I)$ and the I-dependence of F_0 yields an insignificant correction to the nucleation frequency. In the following, as in our past works, we will consider the prefactor F_0 as a constant adjustable parameter. F then takes a noticeable value (arbitrarily assumed to be larger than 1 particle/s/L) only if I exceeds a critical value I_c equal to:

$$\ln I_c = \sqrt{\frac{u}{\ln F_0}} \tag{5}$$

Once the particles have been nucleated, their size may grow or shrink, according to whether their instantaneous radius is larger or smaller than ρ^*. In order to account for this Ostwald ripening effect, which is necessary for a full return to thermodynamic equilibrium of the solid phase, a growth law allowing positive or negative values of $d\rho/dt$ is required[37,38]. The following growth equations:

$$\frac{d\rho}{dt} = \kappa(I^m - \exp\frac{mw}{\rho}) \tag{6}$$

or:

$$\frac{d\rho}{dt} = \kappa(I - \exp\frac{w}{\rho})^m \tag{7}$$

fulfill this requirement. The size dependent term in the right-hand side of the two equations tends to 1 for particles of large size and the two laws are identical for $m = 1$. The characteristics of the growth law (7) for $m \neq 1$ are discussed in the Supporting Information document (SI, Section S1), in which it is shown that it does not allow a return to thermodynamic equilibrium in the absence of seeds. For this reason, only the growth law (6) will be considered in the following.

Apart from the nucleated particles, we assume that N_s seeds (per litre of solution) of the same mineral are introduced in the aqueous solution with an average initial radius ρ_{s0}. These seeds may grow or shrink following the same growth law as the nucleated particles. At each time t their fate thus depends on the value of their radius ρ_s relative to $w/\ln I$ (see equation 6). If large seeds are present ($\rho_s \gg w/\ln I$), their size always grows and their number does not vary. As a first approximation, we will consider that all seeds have the same initial radius, which means that their size distribution function is infinitely narrow. This point is discussed in Section V.

Both the nucleation/growth of particles and the growth of seeds consume the monomers contained in the aqueous solution. A each time t, one may estimate the concentration Q_p and incremental concentration Q_s of growth units contained in the former and the latter, respectively, and thus the saturation state of the aqueous solution, taking into account speciation effects in solution. While the formalism to describe these complex processes has a wider applicability, in all subsequent applications, we will assume (i) that a single type of aqueous ion is relevant, as it occurs for amorphous silica precipitation at neutral pH, for example, (ii) that the mineral has a stoichiometry coefficient equal to 1 relative to this ion, and (iii) that the aqueous solution is diluted enough (activity coefficients equal to 1). In that case, the relationship between I, Q_p and Q_s reads $I = I_0 - (Q_p + Q_s)/K$. All quantities will be referred to 1L of solution.

The equations of nucleation and growth depend on I which, itself depends on Q_p and Q_s through highly non-linear equations which have to be solved in a coupled way. A method of discretization of the time scale is used. In each time increment, a new class of particles is nucleated if $I > I_c$, and the sizes of previously nucleated particles and of seeds are updated. If the particle size inside a given class becomes less that one monomer, this class is destroyed. I is then estimated for the next time increment.

Such an approach provides coupled information on the state of the aqueous solution and on the particle population at each time, which may be compared to experimental solution and particle characterizations. It relies on several parameter values related to nucleation (surface energy σ and prefactor of the nucleation rate F_0) and growth (growth constant κ and m exponent). Our past experience[27,28] shows that the simulation results are usually very sensitive to the values of σ—because the nucleation barrier scales with σ^3— and of κ—because it largely determines the time necessary for a return to thermodynamic equilibrium. At variance, several orders of magnitude on F_0 weakly affect the time scale of the precipitation dynamics.

In the two following sections, we will reveal the generic characteristics of the precipitation process, by allowing the nucleation and growth parameters and the precipitation conditions to freely vary. Only in Section VI will a realistic modelling and a comparison with experimental results be performed.

III. LIMITING CASES

We first describe how the system evolves in the two limiting cases where seeds are either present without nucleation (Section III A), or absent (Section III B).

A. Seed growth in the absence of nucleation

Figure 1 shows the time evolution of the saturation state of the aqueous solution for various values of the growth constant κ (left panel), of the initial saturation state of the aqueous solution I_0 (medium panel) and of the growth exponent m (right panel).

In all cases $I(t)$ decreases and tends toward 1 as time passes, which states that thermodynamic equilibrium is approached. The evolution becomes faster as κ, I_0 or m increase. The final seed radii $\rho_{s\infty}$ increase with I_0, and, since N_s seeds share the available number of monomers of

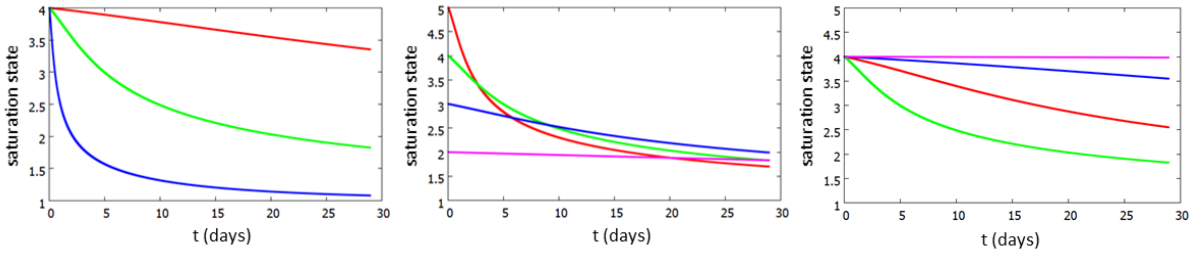

FIG. 1: Time evolution of the saturation state of the aqueous solution when only seed growth is authorized. Reference simulation set-up: $I_0 = 4$, $m = 5$, $\kappa = 10^{-16}$ m/s, ρ_{s0}=30 nm, $N_s = 10^{14}$ seeds/L. Left panel: time dependence for three κ values ($\kappa = 10^{-17}$ (red), 10^{-16} (green) and 10^{-15} (blue)). Medium panel: time dependence for four initial over-saturations (I_0= 5 (red), 4 (green), 3 (blue) and 2 (pink)). Right panel: time dependence for four m exponents ($m = 5$ (green), 4 (red), 3 (blue) and 1 (pink)). The green curves in the three panels correspond to the same simulation conditions.

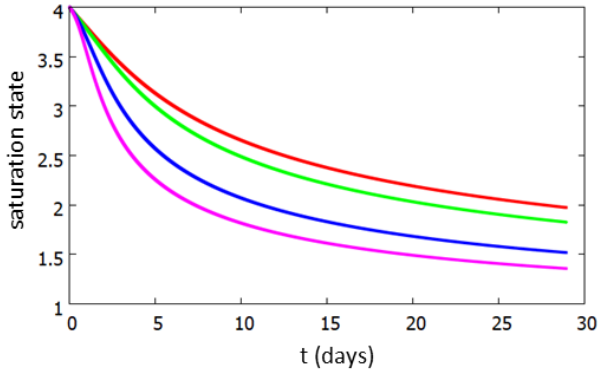

FIG. 2: Time evolution of the saturation state of the aqueous solution when only seed growth is authorized, for four distributions of seeds possessing a constant initial total surface area $N_s * \rho_{s0}^2$. Red curve: ρ_{s0}=30 nm, $N_s = 10^{14}$ seeds/L. Green curve: ρ_0=20 nm, $N_s = 2.25{*}10^{14}$ seeds/L. Blue curve: ρ_{s0}=10 nm, $N_s = 9. * 10^{14}$ seeds/L. Pink curve: ρ_{s0}=5 nm, $N_s = 36 * 10^{14}$ seeds/L. Simulation set-up: $I_0 = 4$, $m = 5$, $\kappa = 10^{-16}$ m/s.

the solution, $\rho_{s\infty}$ is a decreasing function of N_s. $\rho_{s\infty}$ may reach widely different values. Depending on the growth parameters and initial conditions, seeds may hardly grow or display a large size increase.

In the literature, it is often implicitly assumed that the relevant quantity which fixes the time evolution of the system is the total seed area. However, since the equations which couple I and Q_s are particularly simple when only seed growth takes place (N_{Av} the Avogadro number):

$$\frac{dI}{dt} = -\frac{dQ_s}{Kdt} = -\frac{4\pi N_s \rho_s^2 \kappa}{KN_{Av}}(I - \exp\frac{w}{\rho_s}) \qquad (8)$$

it is readily seen that the total seed area $4\pi N_s \rho_{s0}^2$ is the parameter which determines the evolution of I, only when (i) the seeds are large ($w/\rho_s \ll 1$) and (ii) when one may replace ρ_s in the right-hand-side of the equation by ρ_{s0}, which means that the seed size variations are weak ($\delta\rho_s/\rho_s \ll 1$). In most cases however, this is not the case, as shown in the example of Figure 2.

Let us remark that, contrary to what one might expect, in the absence of nucleation $I(t)$ is unable to reach the value $I = 1$. Its decrease stops at some plateau value I_p when $w/\ln I$ and the instantaneous seed radius ρ_s become equal. At that point, I_p and the seed radius ρ_s are linked by the condition $\rho_s = w/\ln I_p$ and the equation of conservation of matter:

$$N_s \frac{4\pi(\rho_{s0}^3 - \rho_s^3)}{3vN_{Av}} = K(I_0 - I_p) \qquad (9)$$

Any further decrease of I would induce seed dissolution (Ostwald ripening effect), which would then increase $I(t)$. A dynamic equilibrium is thus established at $I = I_p \neq 1$. Let us note that the two conditions which link ρ_s and I_p have for consequence that I_p is a decreasing function of N_s. If the seeds display some size dispersion, the smallest seeds may eventually dissolve (Ostwald ripening effect) and only the biggest seeds survive to block the evolution of $I(t)$.

To summarize, the evolution of the saturation state of the aqueous solution is all the faster as I_0, κ or m are larger. However, a full return to thermodynamic equilibrium is not possible as long as no nucleation takes place. The total seed area is the relevant parameter which drives the time evolution of the system only for large seeds ($w/\rho_s \ll 1$) and under the condition of weak radius variations $\delta\rho_s/\rho_s \ll 1$.

B. Nucleation and growth in the absence of seeds

In our past studies[28,29], we have described the generic characteristics of the precipitation of particles in a closed medium, induced by an initial over-saturation of the aqueous solution. We briefly recall them in the following.

When the nucleation frequency is large (large F_0 or small surface energy σ values), $I(t)$ displays a fast initial decrease followed by a quasi-plateau, before the final decrease towards 1 takes place and thermodynamic equilibrium is reached. In contrast, when growth prevails on

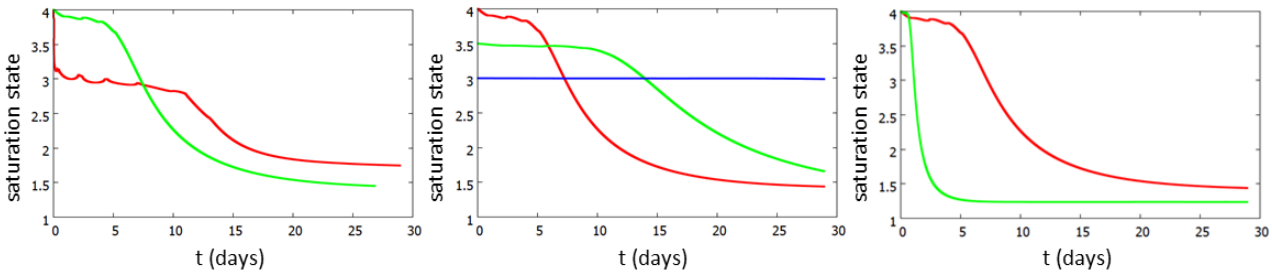

FIG. 3: Time evolution of the saturation state of the aqueous solution in the absence of seeds. Left panel: Evolution for initial $I_0 = 4$ and two F_0 values (red curve: $F_0 = 10^{25}$ particles/s/L; green curve: $F_0 = 10^{19}$ particles/s/L). Medium panel: Evolution as a function of the initial over-saturation I_0= 4, 3.5 and 3 (red, green, and blue, respectively). Right panel: Evolution as a function of the growth constant κ (red curve: $\kappa = 10^{-16}$ m/s ; green curve: $\kappa = 10^{-15}$ m/s). Unless otherwise specified, simulation set-up: $F_0 = 10^{19}$ particles/s/L, $\sigma = 33.3$ mJ/m^2, $m = 5$, $\kappa = 10^{-16}$ m/s.

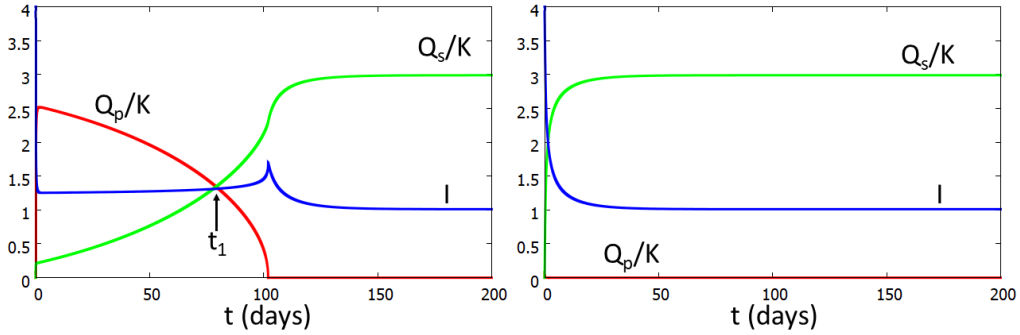

FIG. 4: Time evolution of the saturation state of the aqueous solution (blue curves) and of the precipitated amounts (normalized to K) in the secondary particles (Q_p/K red curves) and in the seeds (Q_s/K green curves), for two values of the growth constant $\kappa = 1.3 * 10^{-15}$ m/s (left panel) and $\kappa = 1.4 * 10^{-15}$ m/s (right panel). Simulation set-up: $I_0 = 4$, $\sigma = 33.3$ mJ/m^2, $m = 5$, $F_0 = 5 * 10^{20}$ part./s/L, ρ_{s0}=30 nm, $N_s = 10^{14}$ seeds/L.

nucleation, I first remains quasi constant before its final decrease. There is no discontinuity between these two behaviors. They are illustrated in Figure 3 (left panel).

In both cases, in the plateau regime, a dynamic equilibrium is established between two opposing forces: on the one hand, nucleation and nucleus size growth impoverish the aqueous solution in monomers; on the other hand the redissolution of particles which become under-critical gives back monomers to the solution. These two forces nearly compensate each other in the plateau regime, but with small time lags responsible for the small oscillations of I. In a number of works, because, either they observe an initial saturation plateau[18,19,39] or they detect no particles during a given amount of time[25], authors refer to the existence of an induction period before the beginning of nucleation. In the framework of crystal growth theory, induction times are produced by non-stationary nucleation processes[34,40]. In our previous study on silica precipitation, we had shown that the non-stationary nucleation theory could not account for the saturation plateau characteristics that we had found. In the present case, the saturation state plateau corresponds to a competition between nucleation/growth/dissolution processes, as described in details in ref.[28,31].

Figure 3 (medium panel) shows that the plateau duration strongly increases for lower values of I_0. This effect clearly manifests itself in Rothbaum and Röhde experiments on amorphous silica nanoparticle synthesis[18]. For example, at 30°C, the plateau length increased from approximately 3 minutes at I_0=5, to 40 mn at I_0=4 and 500 mn at I_0=3, and this dependence was well accounted for by the present formalism[31]. In contrast, the plateau duration becomes shorter when growth is favored over nucleation, whether due to an increase of the growth constant (Figure 3 right panel) or of the m exponent (not shown). In all cases, the shorter the plateau, the faster the return to thermodynamic equilibrium.

IV. GLOBAL SYSTEM DYNAMICS

This section which reveals how the state of an initially over-saturated aqueous solution evolves in the presence of seeds contains the most important results of our study. It highlights two generic growth scenarios, and analyses how they compete as a function of the nucleation/growth parameters and the characteristics of the seeds.

A. Existence of two scenarios

We first focus on the time evolution of the saturation state I of the aqueous solution, of the concentration of monomers Q_p in the nucleated particles (henceforth called 'secondary particles') and of the incremental concentration of monomers Q_s deposited on the seeds. Since, under the present simplifying assumptions $I = I_0 - Q_p/K - Q_s/K$, the results are more conveniently displayed in the figures by the time evolution of Q_p/K and Q_s/K which can be represented on the same scale as I. The starting parameter set-up is chosen close to that determined in our previous study of amorphous silica precipitation in the absence of seeds[31], and a moderate amount of seeds ($N_s = 10^{14}$/L) of initial radius ρ_{s0}=30 nm is considered. Then the parameters are varied to more generally exemplify the possible behaviors that may be encountered during the synthesis of nanoparticles.

Figure 4 shows the time evolution of I, Q_p/K, and Q_s/K for two values of the growth constant κ. The relative values of Q_p and Q_s are drastically different in the two graphs. In the right panel, the variation of I is quasi-entirely due to seed growth. Q_p is vanishingly small, although nucleation exists as long as I remains larger than I_c (equal to 1.98 in this simulation). However, the nuclei do not succeed in growing and they have all disappeared in about $t = 100$ days. The $I(t)$ curve would be nearly identical if nucleation was absent ($F_0 = 0$).

In the left panel of Figure 4, the opposite trend is found in the first stage of precipitation. Due to the large value of F_0, there is an outburst of nuclei, which induces a rapid decrease of I. The amount of matter in the secondary particles Q_p largely exceeds Q_s, up to a characteristic time named t_1 (defined by the equality of Q_p and Q_s), here equal to $\approx$ 80 days. Beyond t_1, Q_p decreases and then vanishes. As seen in Figure 4, although I remains quasi constant during a long period of time, there is a constant exchange of matter between the secondary particles and the seeds, mediated by the aqueous solution. This illustrates the fact that nucleation/growth of secondary particles and seed growth are coupled processes. In the closed system conditions assumed here, both rely on the availability of the same monomers in the aqueous solution.

The decrease of Q_p is due to the Ostwald ripening process in which the smallest particles decrease in size for the benefit of the largest ones. Since the nuclei never reach a size larger than that of the seeds, there is transfer of matter from them to the seeds via the aqueous solution. From a mathematical viewpoint, such a process is allowed by the size dependent $\exp w/\rho$ term in the growth law. The seeds have a radius ranging from 30 nm at $t = 0$ to 73 nm in the long term. Whatever t, their radius is such that $I - \exp(w/\rho) > 0$. Thus they never dissolve and their number remains constant. Things would be different if their radius was much smaller (see discussion in Section IV C).

To summarize, in the presence of seeds, two processes contribute to the decrease of I and the recovery of thermodynamic equilibrium: the nucleation and growth of secondary particles and the growth of seeds. These two processes are in competition to consume the monomers of the supersaturated aqueous solution. This competition leads to two scenarios of precipitation, in which either the former of the latter process prevails.

B. Growth diagrams

It is noteworthy that the two scenarios displayed in Figure 4 are obtained for very close values of the growth constant κ, equal to $1.3 * 10^{-15}$ m/s and $1.4 * 10^{-15}$ m/s, respectively. This tells that the transition between the two regimes (henceforth named "S" for seed growth prevalence and "N" for secondary particle prevalence) is quite abrupt, and thus can be localized with a good precision in the multi-dimensional space of the simulation parameters.

Figure 5 (top panel) displays the localization of this transition in a plot $\{\log \kappa, \log F_0\}$. The transition line is quasi-linear with a slope approximately equal to 1, thus obeying an equation $\kappa_c \propto F_{0c}$ with a positive coefficient of proportionality. From a point located on the transition line, increasing F_0 favors nucleation and thus leads to the "N" domain. In contrast, increasing κ leads to the "S" domain. Actually large κ values do favor both seed growth and new particle growth, but Figure 5 proves that the first process prevails.

In the "N" region of the growth diagram, the time t_1 at which Q_p becomes equal to Q_s is quasi independent of F_0, as shown by the horizontal black lines in the top panel Figure 5. This means that the triangular region of the diagram limited by the transition line and a given t_1 line recovers a "S" character, but only for times larger than t_1. This characteristic time is strongly dependent on the growth constant value, as represented in Figure 5 (medium panel). When κ increases, the amount of matter deposited in the seeds grows more quickly and the Q_s curve reaches the Q_p one at shorter times. This explains the negative slope of the t_1 curve in the Figure. More specifically, the dependence of $\log t_1$ on $\log \kappa$ is quasi linear with a slope close to -1, meaning that $t_1 \propto 1/\kappa$.

The localization of the transition line depends on the initial value of the saturation state I_0, as shown in Figure 5 (bottom panel). When I_0 increases, the size of the seed domain "S" decreases. This result may be explained by the lowering of the nucleation barrier (equation 3) which favors nucleation.

C. Influence of the seed characteristics

The seed characteristics (their number N_s and initial radius ρ_{s0}) have a sound influence on the position of the

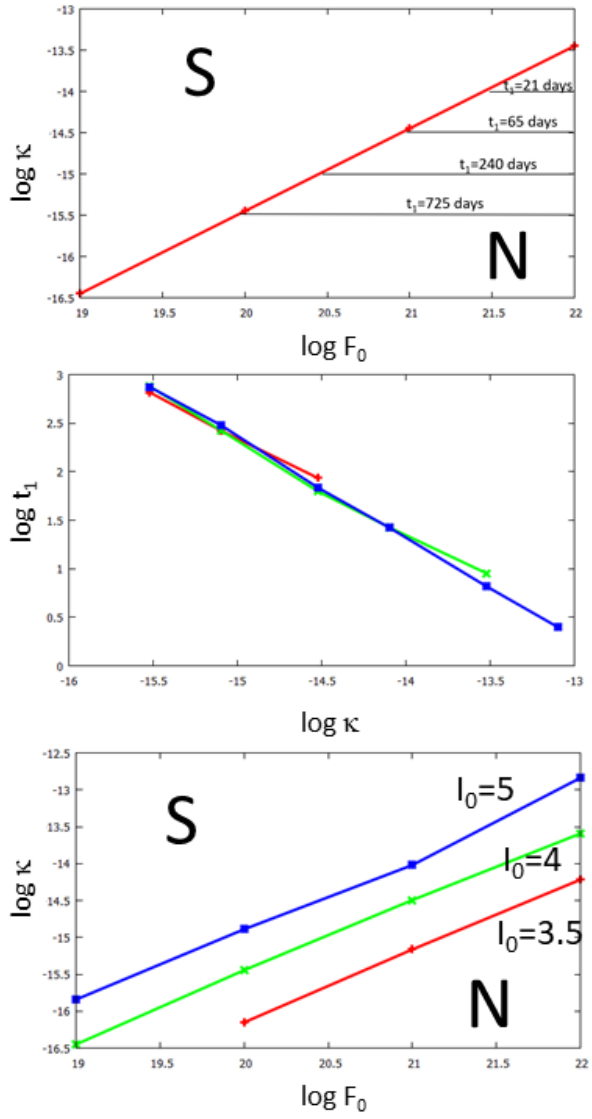

FIG. 5: Top: Red curve: localization of the transition lines in a $\{\log\kappa$ (m/s), $\log F_0$ (part./s/L)$\}$ plot between the "S" domain in which seed growth is dominant and the "N" domain in which the production of new particles prevails. The lines of constant t_1 values are represented in black. Medium: variations of $\log t_1$ (days) as a function of $\log\kappa$ (m/s). The red, green and blue curves refer to three values of F_0 ($F_0 = 10^{21}$, 10^{22} and 10^{23} part./s/L, respectively). Bottom: localization of the transition line for three initial over-saturation values ($I_0 = 5, 4$ and 3.5). Simulation parameters: $I_0 = 4$, $\sigma = 33.3$ mJ/m^2, $m = 5$, $N_s = 10^{14}$ seeds/L, ρ_{s0}=30 nm.

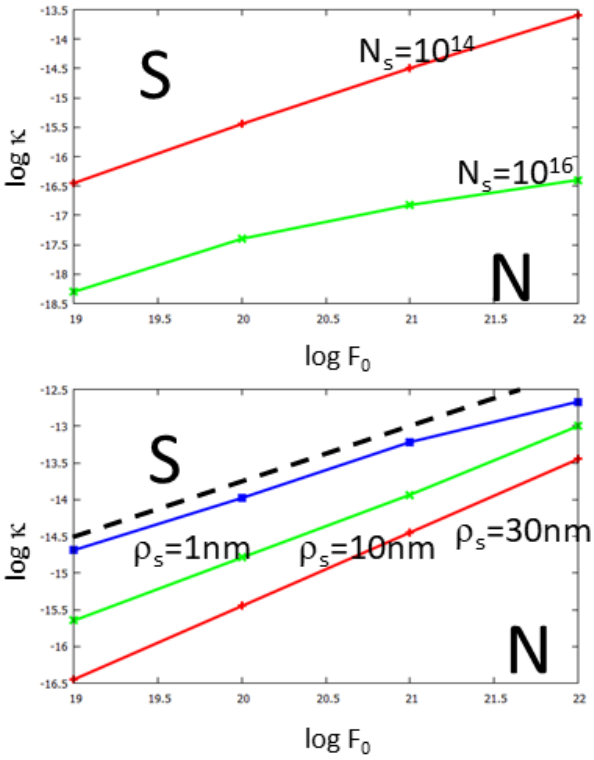

FIG. 6: Same as Figure 5. Top: for two seed numbers $N_s = 10^{14}$ and 10^{16} seeds/L . Bottom: for three values of the seed initial radius ρ_{s0}=30 nm, 10 nm and 1 nm. The dashed line indicates the critical radius under which all seeds immediately dissolve, equal to 5.62 Å in the present simulation. Simulation parameters, unless otherwise specified: $I_0 = 4$, $\sigma = 33.3$ mJ/m^2, $m = 5$, ρ_{s0}=30 nm, $N_s = 10^{14}$ seeds/L.

transition line in the growth diagrams. It may be expected that the "S" region will shrink when these two parameters—that is the total surface area of the seeds—become smaller and smaller. However, we show in the following that the effect of decreasing N_s or decreasing ρ_{s0} are not equivalent.

Figure 6 (top panel) displays the regions of prevalence of the "N" and "S" phases for two values of the seed number N_s. As expected, when N_s decreases, the seed prevalence weakens and the "N" region expands. Eventually, the "S" domain completely disappears when $N_s \to 0$. A decrease of the seed radius also leads to a shrinking of the "S" domain as shown in Figure 6 (bottom panel), for three values of ρ_{s0}. However, contrary to the continuous shift of the dividing line when $N_s \to 0$, there is a critical ρ_{s0} radius below which the "S" domain suddenly vanishes (dashed line in Figure 6).

A first estimate of this critical value is obtained when at $t = 0$ ρ_{s0} is equal to the critical nuclei radius , i.e. when $\rho_{s0} = w/\ln I_0$. Indeed, any subsequent decrease of $I(t)$ makes the seeds even more under-critical and thus induces seed dissolution, as a consequence of the Ostwald ripening effect. This critical radius may vary in a quite extended range, since it depends on the initial saturation state of the aqueous solution I_0, on the surface energy σ and the formula unit volume v, via the w parameter $w = 2\sigma v/(k_B T)$ (see equation 2). For example, in the case of silica[31] ($\sigma = 33.3$ mJ/m^2, $v = 48.15 * 10^{-30}$ m^3, see section VI), ρ^c_{s0} varies from 0.34 nm at $I_0 = 10$ to 1.14 nm at $I_0 = 2$, while for calcite particles[30] ($\sigma = 97$ mJ/m^2, $v = 61.3 * 10^{-30}$ m^3), the corresponding values

are 1.27 nm and 4.23 nm, respectively.

Actually, this very restrictive condition $\rho_{s0} < w/\ln I_0$ is not mandatory to observe seed dissolution. In the "S" domain, it may happen that the inequality is not fulfilled at $t = 0$ but that, at a later time t, the seed radius becomes smaller than the *instantaneous* critical nucleus radius $\rho^*(t) = w/\ln I(t)$. An example is given in Figure 7. As mentioned previously (Section III A), when only seed growth takes place, the saturation state of the aqueous solution never reaches the value $I = 1$ but remains stuck on a plateau value $I = I_p$ for which $\rho_s = w/\ln I_p$. When nucleation occurs, in the "S" region of the growth diagram, the saturation state also displays a plateau. However, if I_p happens to be larger than the critical value for nucleation I_c, the duration of the plateau remains finite. Due to nucleation, $I(t)$ decreases, which breaks the plateau dynamic equilibrium and leads to total seed dissolution. Beyond this time noted t_{dissol} in Figure 7 (top panel), the remaining time evolution of the system is driven by the growth of the secondary particles. For this scenario to exist, the initial seed radius has to be smaller than $w/\ln I_c$.

The existence of seed dissolution is also dependent on the number N_s of seeds. We had noted in Section III A that the two conditions which link ρ_s and I_p have for consequence that I_p is a decreasing function of N_s. Consequently, at constant ρ_{s0} value, there generally exists a critical value N_s^c at which $I_p = I_c$. For $N_s > N_s^c$, $I_p < I_c$ and no further nucleation may take place, while for $N_s < N_s^c$ seed dissolution occurs. For $N_s = N_s^c$ (equal to $\approx 2.5 * 10^{19}$ seeds/L in Figure 7 (bottom panel)), the time t_{dissol} at which all seeds have disappeared is infinite. It decreases when N_s is further increased. N_s^c is independent on the growth constant κ. It only weakly varies with F_0, because its dependence involves $\sqrt{\ln F_0}$. Its largest variations are linked to the value of the initial saturation state of the aqueous solution I_0. It decreases as the initial over-saturation gets smaller.

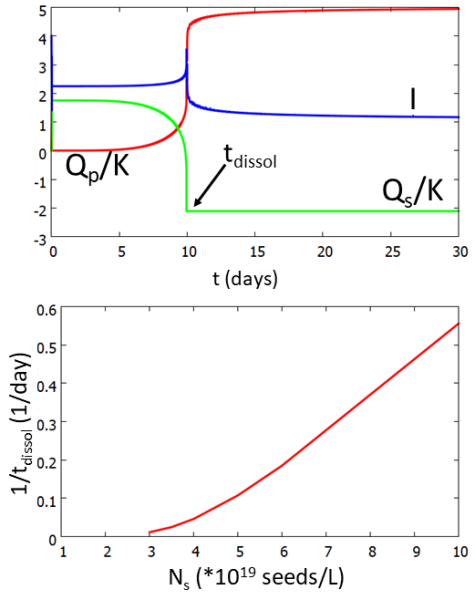

FIG. 7: Top: Time evolution of the saturation state of the aqueous solution (blue curves) and of the precipitated amounts (normalized to K) in the secondary particles (Q_p/K red curves) and in the seeds (Q_s/K green curves) evidencing seed dissolution after a characteristic time $t_{dissolv}$. When the seed radius becomes less than ρ_{s0}, Q_s (defined as the amount of matter deposited on the seeds) becomes negative. The maximum negative value it takes is equal to the number of monomers initially present in all seeds, equal to $4\pi N_s \rho_{s0}^3/(3vN_{Av})$. Parameter set-up: $I_0 = 4$, $\sigma = 33.3$ mJ/m^2, $m = 5$, $F_0 = 10^{23}$ part/s/L, $\kappa = 10^{-15}$ m/s, $N_s = 5 * 10^{19}$ seeds/L and ρ_{s0}=0.8 nm. Bottom: variation of $1/t_{dissol}$ as a function of N_s for the same parameter set-up

.

V. DISCUSSION

The present formalism has been devised to account for the kinetic effects which accompany the synthesis of nanoparticles in the presence of seeds of the same chemical composition, in a closed, initially over-saturated, medium, thus mimicking experiments performed in academic or industrial laboratories.

We have found that, in the presence of seeds, two processes contribute to the decrease of I and the return to thermodynamic equilibrium: the growth of seeds and the nucleation and growth of secondary particles which are coupled since they consume the same monomers of the aqueous solution. Their competition leads to two scenarios of precipitation, in which either the formation of secondary particles or seed growth prevails. It relies on the possible exchange of matter between them via the aqueous solution. The account of Ostwald ripening effects, thanks to the use of a size-dependent growth law, is mandatory to unveil these complex processes. The transition between the two scenarios is abrupt, so that one can localize it with a good precision in the multi-dimensional space of the simulation parameters. In the $\{\log\kappa, \log F_0\}$ growth diagrams of Section IV B, well-defined regions of "S" or "N" character are evidenced, whose sizes depend on the initial over-saturation I_0, and on the seed characteristics. To experimentally determine which scenario is relevant, the only reliable evidence may come from a careful characterization of the particle size distribution (by TEM or other methods). In this respect, the analysis of the aqueous solution characteristics alone (the shape of the time dependence of I) is clearly insufficient.

Contrary to intuitive—and most of the time implicit—assumption, the total surface area of the seeds initially put in the aqueous solution cannot be considered as the sole seed parameter which drives the evolution of the system. In the limit of large surface areas (large number of seeds and/or large initial radius), it is correctly indicative of the qualitative trends to be expected. However, its decrease may lead to a progressive or a discontinuous

reduction of the "S" region, depending on whether this is due to a reduction of the seed number or of the seed radius.

The analysis performed in Section IV assumes that all seeds have the same size. This is a very unrealistic assumption, since it is impossible to synthesize nanoparticles—and thus obtain seeds—without some size dispersion. The TEM images of witherite seeds in Ref.[41] for example clearly reveal this point. In order to perform realistic simulations for each specific case, one needs information on the size distribution function of the seeds. Here, in order to test the robustness of the results of Section IV, we have performed an additional simulation in which, instead of assuming equal size for all seeds, we have considered a simple bimodal distribution which preserves the total number of seeds and their average radii. We have used the same parameter set-up as in Figure 5, and replaced the initial seed characteristics: $N_s = 10^{14}$ seeds/L and $\rho_{s0} = 30$ nm, by the distribution: $N_{s1} = N_{s2} = 0.5 * 10^{14}$ seeds/L, ρ_{s1}=45 nm, and ρ_{s2}=15 nm. We have found that the time evolution of I displays the expected two scenarios, with a transition between them only slightly shifted towards lower κ values (see SI, Figure S4). As an additional feature, in the long term, in the "S" domain, the seeds of smaller size get dissolved in favor of the larger ones as a result of Ostwald ripening (SI Figure S5). Although simplistic, this test suggests that, at least in the regimes in which all seeds do not dissolve, the generic scenarios obtained in Section IV are qualitatively robust.

The complexity of the precipitation kinetics results from the coupling of the highly non-linear equations which drive nucleation and growth processes in a closed medium. It is quite obvious that simple rate equation formalisms, such as those currently used in water-rock interaction codes, for example in KINDIS[42], KIRMAT[43], CRUNCHFLOW[44] and so on, are unable to account for this richness. The use of a single equation of the type:

$$R = k(I^m - 1)^{m'} \tag{10}$$

where R represents the rate of precipitated matter and k a rate constant, cannot account for the fate of two populations of particles (the secondary particles and the seeds) obeying different kinetic laws. It cannot predict the competition between them, nor the existence of two growth scenarios, nor an abrupt transition between them. Its major drawback is its inability to account for Ostwald ripening effects which are at the basis of the competition between the secondary particles and the seeds. The application to the synthesis of amorphous silica nanoparticles in the conditions of Ref.[11] in the next section clearly highlights this failure.

Besides the application to specific synthesis conditions, the interest of the present approach is to draw the attention to the possible role of the nucleation and growth of secondary particles in seed-mediated syntheses. If the goal is to obtain a monodispersed distribution of nano- or micro-particles, the conditions of synthesis have to be set-up in such a way that the system locates itself into the "S" region of the growth diagrams. Possible strategies include an increase of the seed number or radius, or a decrease of the initial saturation state of the aqueous solution. As shown in Section IV B, limiting values of these three parameters are determined by the nucleation and growth parameters of the mineral under consideration: the prefactor of nucleation F_0, the mineral surface energy σ and the growth parameters κ and m.

VI. APPLICATION TO THE SYNTHESIS OF AMORPHOUS SiO_2 NANOPARTICLES IN THE PRESENCE OF SEEDS.

Because the precipitation of amorphous silica nanoparticles occurs in numerous industrial and natural processes, its mechanism has been the subject of intensive research[18–20,24,25,39,45–47]. Results obtained in laboratory, in the absence[10,18,24,25] or presence[10,11,16,17] of seeds have yielded precious information on the role of temperature, pH, ionic strength and initial over-saturation. In a previous study[31], we have successfully interpreted the numerous and detailed results of Rothbaum et al.[18] and Tobler et al.[24] in the absence of seeds with the formalism described in Sections II and III B. We have selected the work by Fernandez et al.[11] to validate our formalism when applied to seed experiments, since it complements our previous work together with exemplifying the two cases in which either seeds or newly formed particles prevail.

Roerdink et al.[10] and Fernandez et al.[11] experiments have been performed under the conditions specified in Table 1, with three seed families characterized by a High, a Medium or a Low surface area (in the following HSA, MSA and LSA, respectively). The seed radii and numbers were estimated from their total surface area and mass under the assumption that all seeds have a spherical shape and identical sizes, knowing the molar mass (Mm=60.08 g/mole) and molar volume (Vm=290*10^{-7} m^3) of SiO_2.

TABLE 1: Seed characteristics in the HSA experiment of Roerdink et al. and in the HSA, MSA and LSA of Fernandez et al. experiments[10,11]: M their mass per litre of solution and S their associated total surface area, ρ_{s0} their initial radius, N_s their number per litre of solution. The experiments were performed at T=20°C, pH=7.3 and initial SiO_2 concentration in the aqueous solution 5.3 mM/L.

	HSA	MSA	LSA
M (g/L)	10	16	16
S (m^2/L)	495	2.17	1.25
ρ_{s0}	29 nm	11.4 μm	20.1 μm
N_s (seeds/L)	4.6*10^{16}	13.2*10^8	2.47*10^8

The evolution of the saturation state of the solution displayed in Figure 1A of Fernandez et al.' work[11], was

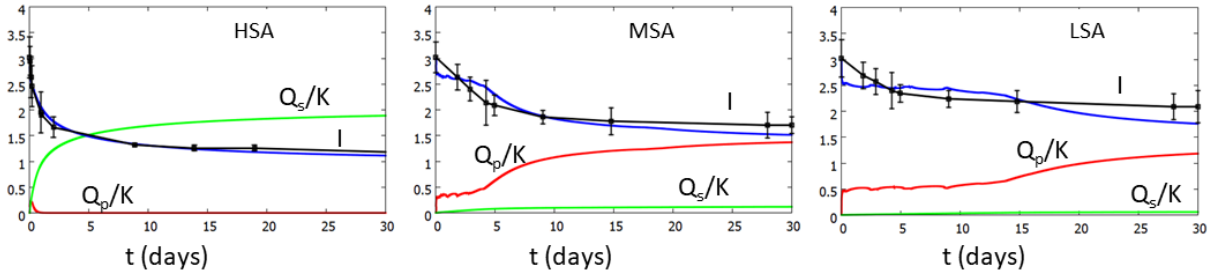

FIG. 8: Simulated evolution of the saturation state of the aqueous solution in the conditions of the HSA, MSA and LSA (from left to right, respectively) experiments of Fernandez et al.[11], with error bars given in their work (black lines). The blue lines represent the best fits that have been obtained with $F_0 = 10^{24}$ part./s/L and $\kappa = 0.7 * 10^{-17}$ m/s for HSA; $F_0 = 10^{24}$ part./s/L and $\kappa = 1.5 * 10^{-17}$ m/s for MSA; and $F_0 = 10^{25}$ part./s/L and $\kappa = 0.7 * 10^{-17}$ m/s for LSA. The red and green lines give the Q/K values of the newly created particles and the seed growth. Other parameter values: $\sigma = 33.3$ mJ/m^2, $m = 6$

interpreted by the authors within a rate equation model:

$$R = kS(I-1)^m \tag{11}$$

R being the concentration of precipitated silica per second and $m = 3.5$. They got an approximate agreement between the model predictions and the experimental results. However the initial values of R/S, equal to $10^{-9.48}$, $10^{-8.62}$ and $10^{-8.47}$ moles/m^2/s for HSA, MSA and LSA, respectively, according to the authors, correspond to one order of magnitude difference in the rate constant k between HSA and LSA, showing the inadequacy of the model.

The same problem arises if one tries to reproduce these results within an approach which only considers seed growth, as described in Section III A. Good agreement with experimental results may be obtained, as shown in Figure S6 in the SI. However, the best fits yield growth constants equal to 0.7*10^{-17} m/s, 1.7*10^{-16} m/s and 1.3*10^{-16} m/s for the HSA, MSA and LSA experiments, respectively. More generally, whatever the value chosen for m, the κ value necessary to reproduce the MSA and LSA curves has to be of the order of 20 times larger than that for HSA.

These two failures in reproducing the time evolution of the aqueous solution point to the necessary account of the nucleation of secondary particles. This necessity is further confirmed by additional data given by Roerdink et al. (in their SI)[10] who, starting from the same aqueous solution concentration under the same thermodynamic conditions, find a nearly as rapid decrease of the saturation state of the solution *in the absence of seeds*.

Applying our global approach, we have searched the simulation set-up which allows reproducing the time evolution of I in the three experiments of Fernandez et al.[11]. We have used as input parameters: $K = 1.7510^{-3}$ the solubility product of amorphous silica at ambient temperature, $v = 48.1510^{-30}$ m^3 the molecular volume in the solid phase, $m = 6$ the exponent growth law determined in our previous study, and $\sigma = 33.3$ mJ/m^2. Let us note that this value, also derived from our previous work is very low, especially as compared to typical values measured by thermodynamic methods on hydrated silica[48–50]. However, here, σ is rather a fitting parameter which has to be consistent with the CNT assumption[36]. The latter simplifies the nucleation process by assuming that a single barrier has to be overcome, while multiple-step nucleation processes may involve precursor phases or pre-nucleation clusters which, in an effective way accelerate the formation of new particles[51,52]. When these more complex processes take place, the CNT can only account for them in an effective way by a decrease of the σ parameter which lowers the nucleation barrier. It is noteworthy that σ parameters extracted from nucleation experiments with the help of CNT are indeed very low[53].

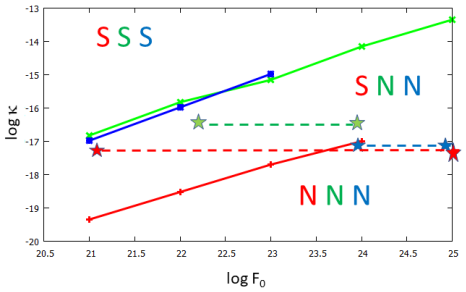

FIG. 9: Localization of the transition lines between the "S" domain in which seed growth is dominant and the "N" domain in which production of new particles is dominant in a $(\log\kappa, \log F_0)$ plot. The red, green and blue curves refer to the conditions HSA, MSA and LSA of Fernandez et al.[11]. The dotted lines indicate the range of values for which a reasonable fit could be obtained. Simulation set-up: $I_0 = 3$, $K = 1.7510^{-3}$, $\sigma = 33.3$ mJ/m^2, $m = 6$.

We first show in Figure 8 the best fits separately obtained for each experiment, and with dotted lines in the stability diagram of Figure 9 the range of parameter values which allow obtaining a reasonable fit for them. We had noted in the past that several orders of magnitude on F_0 weakly affect the time scale of the precipitation kinetics. Nevertheless, the $\log F_0$ range is particularly large for HSA conditions in which the shape of the I curve nearly

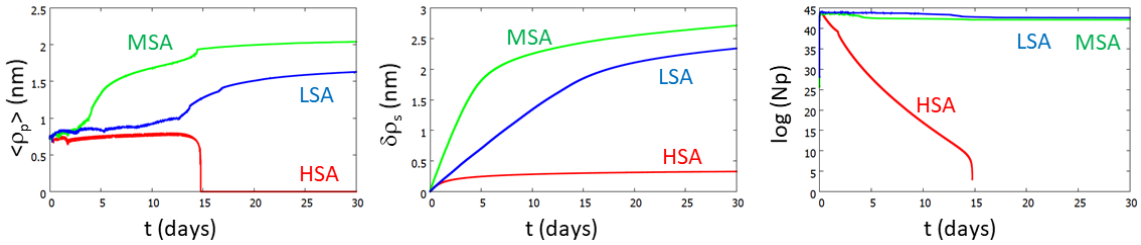

FIG. 10: From left to right: Time evolution of average radius of the secondary particles ρ_p(nm), of the incremented radius of the seeds $\delta\rho_s$(nm) and of the concentration of secondary particles (log scale, per liter). The red, green and blue curves refer to the conditions HSA, MSA and LSA of Fernandez et al.[11]. Same simulation set-up as in Figure 9.

entirely relies on the growth constant value. This is reasonable, since in this case the contribution of nucleation of secondary particles is negligible (vanishingly small Q_p in Figure 8), thus allowing a large range of possible F_0 values. In contrast, the range of F_0 values which allows obtaining good agreement with experiment is narrower for the MSA and LSA conditions, revealing a larger sensitivity to nucleation processes. As a whole, although the best parameter values remain in a quite restricted zone of the stability diagram, we do not find a single set of κ and F_0 values valid for the three cases. This may be due to the fact that seed sizes are not monodispersed, but the parameter dispersion in the growth diagram remains narrow.

Even admitting some uncertainty regarding the precise parameter values, the robust outcome of Figures 8 and 9 lies in the fact that the HSA experiment is driven by seed growth, while the MSA and LSA conditions are in the "N" regime, meaning that nucleation and growth of secondary particles prevail during the time of the experiment. This explains why a purely seed growth approach or a rate equation model are unable to correctly account for the experimental time evolution of the saturation state of the solution.

Additionally, the present simulations provide information on the composition of the solid phase, as a function of time (Figure 10). We find that the seed radii have grown by $\delta\rho_s$=0.33 nm, 2.7 nm and 2.3 nm in the HSA, MSA and LSA experiments, respectively. The first value is close to the value 0.19 nm quoted in reference[11], but the two others are much smaller than the accumulated depths 36.5 and 58 nm quoted for MSA and LSA, respectively. This difference stems for the overall matter contained in the secondary particles, disregarded in the quoted work. During the strong nucleation period, the secondary particles are much more numerous than the seeds. Their radii keep growing in time in the MSA and LSA experiments, while dissolution takes place at approximated t =15 days in the HSA experiment. This overall behavior is consistent with the time evolution of Q_p in the three experiments, shown in Figure 9, but unfortunately there are no direct experimental determination of the particle characteristics to compare to. This discussion recalls that a full understanding of a precipitation experiment, whether in the presence or absence of seeds, not only requires a characterization of the aqueous solution but also of the solid phase, for example via small angle X ray scattering, as in Reference[24] or via TEM imaging.

To summarize, we propose an alternative interpretation of the results of reference[11]. We show that the account of both seed growth and nucleation of secondary particles is mandatory to obtain a fair and well-founded agreement with the experimental results. While in the HSA case, nucleation produces only a small correction, its influence appears to be critical in the MSA and LSA experiments.

VII. CONCLUSION

Considering the widespread use of seeds for the synthesis of nanoparticles in industrial and academic laboratories, we have devised a formalism which accounts for both seed growth and formation of new particles in a closed initially over-saturated aqueous solution. The approach is based on the classical nucleation theory and involves a size-dependent growth law able to produce Ostwald ripening effects. The time evolution of the particle population and of the aqueous solution composition are consistently treated via a feed-back loop. Although the present implementation relies on several simplifying assumptions, it already provides a number of interesting outcomes.

We demonstrate that a strong coupling exists between seed growth and nucleation/growth of secondary particles and that these two processes compete to consume the same monomers of the aqueous solution. This competition relies on the possible exchange of matter between them through the aqueous medium (Ostwald ripening effect), which can only be accounted for by a size-dependent growth law, absent in most water-rock interaction codes. In the multi-dimensional parameter space, regions where one or the other process prevails are well-defined and the transition between them is abrupt. The position of the transition line in $\{F_0, \kappa\}$ plots depends on the initial saturation state, and on the number and size of the seeds. In the general case, the choice of an initial total surface area of the seeds does not fully determine

the orientation of the synthesis, especially in the limit of small surface areas where the two seed characteristics—number and size— play different roles.

We have used this approach to propose an alternative, more founded, interpretation of the experimental results of Fernandez et al.[11] on amorphous silica nanoparticle synthesis. We demonstrate that neither a rate equation approach nor one which neglects nucleation processes can correctly reproduce their results. This stems for the decisive role of the formation of secondary particles on the time evolution of the saturation state of the aqueous solution. The present discussion warns that a full understanding of a precipitation experiment, whether in the presence or absence of seeds, not only requires a characterization of the aqueous solution but also of the solid phase.

The interest of the present approach is to draw the attention to the possible role of nucleation and growth of secondary particles in seed-mediated syntheses and serve as guidelines to experimentalists or industrialists. It stresses the fact that in order to obtain a monodispersed distribution of nano- or micro-particles, the conditions of synthesis—the initial seed number and size and the initial over-saturation of the aqueous solution—have to be set-up in such a way that the system locates itself into the "S" region of the growth diagrams.

VIII. DECLARATION OF COMPETING INTEREST

The authors declare that they have no known competing financial interests or personal relationships that could influence the work reported in this paper.

IX. SUPPORTING INFORMATION

A Supporting Information document is available, free of charge at address... It contains:

- a discussion of the applicability of the growth law 7 to nucleation and growth processes
- a first account of a bimodal size distribution of seeds
- a simulation of amorphous silica precipitation assuming no nucleation.

[1] M. F. Hochella, S. K. Lower, P. A. Maurice, R. L. Penn, N. Sahai, D. L. Sparks, and B. S. Twining, Science **319**, 1631 (2008).
[2] M. I. Carretero and M. Pozo, Applied Clay Science **46**, 73 (2009).
[3] M. I. Carretero and M. Pozo, Applied Clay Science **47**, 171 (2010).
[4] J. C. Védrine, Catalysts **7**, 341 (2017).
[5] X. Huang and M. A. El-Sayed, Journal of Advanced Research **1**, 13 (2010).
[6] Z. L. Wang, Journal of Physics: Condensed Matter **16**, R829 (2004).
[7] J.-P. Jolivet, *Metal Oxide Nanostructures Chemistry: Synthesis from Aqueous Solutions* (Oxford University Press, New York, 2019).
[8] T. K. Sau and C. J. Murphy, Journal of the American Chemical Society **126**, 8648 (2004).
[9] J. Pérez-Juste, I. Pastoriza-Santos, L. M. Liz-Marzán, and P. Mulvaney, Coordination Chemistry Reviews **249**, 1870 (2005).
[10] D. L. Roerdink, S. H. van den Boorn, S. Geilert, P. Z. Vroon, and M. J. van Bergen, Chemical Geology **402**, 40 (2015).
[11] N. M. Fernandez, X. Zhang, and J. L. Druhan, Geochimica et Cosmochimica Acta **262**, 104 (2019).
[12] N. Karapinar, E. Hoffmann, and H. H. Hahn, Water Research **38**, 3059 (2004).
[13] S. Geider, B. Dussol, S. Nitsche, S. Veesler, P. Berthézène, P. Dupuy, J. Astier, R. Boistelle, Y. Berland, J. Dagorn, et al., Calcified Tissue International **59**, 33 (1996).
[14] X. Zhao, G. Lu, and H. Zhu, Journal of Porous Materials **4**, 245 (1997).
[15] E. John, T. Matschei, and D. Stephan, Cement and Concrete Research **113**, 74 (2018).
[16] S.-L. Chen, P. Dong, G.-H. Yang, and J.-J. Yang, Journal of Colloid and Interface Science **180**, 237 (1996).
[17] S. M. Chang, M. Lee, and W.-S. Kim, Journal of Colloid and Interface Science **286**, 536 (2005).
[18] H. Rothbaum and A. Rohde, Journal of Colloid and Interface Science **71**, 533 (1979).
[19] G. A. Icopini, S. L. Brantley, and P. J. Heaney, Geochimica et Cosmochimica Acta **69**, 293 (2005).
[20] C. F. Conrad, G. A. Icopini, H. Yasuhara, J. Z. Bandstra, S. L. Brantley, and P. J. Heaney, Geochimica et Cosmochimica Acta **71**, 531 (2007).
[21] M. Avrami, The Journal of Chemical Physics **7**, 1103 (1939).
[22] M. Avrami, The Journal of Chemical Physics **8**, 212 (1940).
[23] W. A. Johnson, Am. Inst. Min. Metal. Petro. Eng. **135**, 416 (1939).
[24] D. J. Tobler, S. Shaw, and L. G. Benning, Geochimica et Cosmochimica Acta **73**, 5377 (2009).
[25] D. J. Tobler and L. G. Benning, Geochimica et Cosmochimica Acta **114**, 156 (2013).
[26] A. Nielsen, Acta Chemica Scandinavica **13**, 784 (1959).
[27] C. Noguera, B. Fritz, A. Clément, and A. Baronnet, Journal of Crystal Growth **297**, 180 (2006).
[28] C. Noguera, B. Fritz, A. Clement, and A. Baronnet, Journal of Crystal Growth **297**, 187 (2006).
[29] B. Fritz, A. Clement, Y. Amal, and C. Noguera, Geochimica et Cosmochimica Acta **73**, 1340 (2009).
[30] B. Fritz, A. Clément, G. Montes-Hernandez, and C. Noguera, CrystEngComm **15**, 3392 (2013).

[31] C. Noguera, B. Fritz, and A. Clément, Journal of Colloid and Interface Science **448**, 553 (2015).
[32] B. Fritz, A. Clément, G. Montes-Hernandez, and C. Noguera, Chemical Geology **497**, 18 (2018).
[33] A. W. Adamson, *Physical Chemistry of Surfaces* (Interscience Publishers, Chichester, 1960).
[34] I. V. Markov, *Crystal Growth for Beginners: Fundamentals of Nucleation, Crystal Growth, and Epitaxy* (World Scientific, New Jersey, London, Singapore, 1995).
[35] P. W. Schindler (ACS Publications, 1967).
[36] M. Prieto, Mineralogical Magazine **78**, 1437 (2014).
[37] O. Myhr and Ø. Grong, Acta Materialia **48**, 1605 (2000).
[38] L. Ratke and P. W. Voorhees, *Growth and coarsening: Ostwald ripening in material processing* (Springer Science & Business Media, 2013).
[39] S. Carroll, E. Mroczek, M. Alai, and M. Ebert, Geochimica et Cosmochimica Acta **62**, 1379 (1998).
[40] D. Kashchiev, Surface Science **14**, 209 (1969).
[41] V. Mavromatis, K. van Zuilen, B. Purgstaller, A. Baldermann, T. F. Nägler, and M. Dietzel, Geochimica et Cosmochimica Acta **190**, 72 (2016).
[42] B. Madé, A. Clément, and B. Fritz, Computers & Geosciences **20**, 1347 (1994).
[43] F. Gérard, A. Clément, and B. Fritz, Journal of Contaminant Hydrology **30**, 201 (1998).
[44] C. I. Steefel, Software for modeling multicomponent reactive flow and transport. Userâs manual. Lawrence Berkeley National Laboratory, Berkeley (2009).
[45] R. K. Iler, *The colloid chemistry of silica and silicates*, vol. 80 (LWW, 1955).
[46] A. C. Makrides, M. Turner, and J. Slaughter, Journal of Colloid and Interface Science **73**, 345 (1980).
[47] J. D. Rimstidt and H. Barnes, Geochimica et Cosmochimica Acta **44**, 1683 (1980).
[48] J. Mizele, J. Dandurand, and J. Schott, Surface Science **162**, 830 (1985).
[49] S. Brunauer, D. Kantro, and C. Weise, Canadian Journal of Chemistry **34**, 1483 (1956).
[50] G. Alexander, The Journal of Physical Chemistry **61**, 1563 (1957).
[51] D. Gebauer, M. Kellermeier, J. D. Gale, L. Bergström, and H. Cölfen, Chemical Society Reviews **43**, 2348 (2014).
[52] A. Navrotsky, Geochemical Transactions **4**, 34 (2003).
[53] O. Söhnel, Journal of Crystal Growth **57**, 101 (1982).

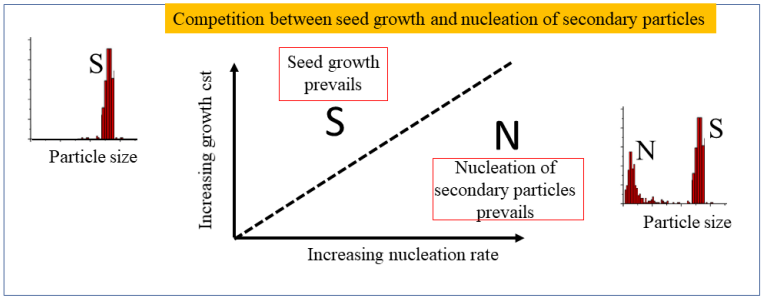
Competition between seed growth and nucleation of secondary particles
S
Particle size
Seed growth prevails
S
N
Nucleation of secondary particles prevails
Increasing growth cst
Increasing nucleation rate
N
S
Particle size